



This is a repository copy of *On improved fail-safe sensor distributions for a structural health monitoring system*.

White Rose Research Online URL for this paper:
<https://eprints.whiterose.ac.uk/190327/>

Version: Published Version

Article:

Wang, T. orcid.org/0000-0002-1271-2641, Barthorpe, R.J., Wagg, D. et al. (1 more author) (2022) On improved fail-safe sensor distributions for a structural health monitoring system. *Data-Centric Engineering*, 3. e27. ISSN 2632-6736

<https://doi.org/10.1017/dce.2022.27>

Reuse

This article is distributed under the terms of the Creative Commons Attribution (CC BY) licence. This licence allows you to distribute, remix, tweak, and build upon the work, even commercially, as long as you credit the authors for the original work. More information and the full terms of the licence here:
<https://creativecommons.org/licenses/>

Takedown



If you consider content in White Rose Research Online to be in breach of UK law, please notify us by emailing eprints@whiterose.ac.uk including the URL of the record and the reason for the withdrawal request.



eprints@whiterose.ac.uk
<https://eprints.whiterose.ac.uk/>

RESEARCH ARTICLE  

On improved fail-safe sensor distributions for a structural health monitoring system

Tingna Wang* , Robert J. Barthorpe, David J. Wagg  and Keith Worden

Dynamics Research Group, Department of Mechanical Engineering, University of Sheffield, Mappin Street, Sheffield S1 3JD, United Kingdom

*Corresponding author. E-mail: twang71@sheffield.ac.uk

Received: 01 November 2021; **Revised:** 22 July 2022; **Accepted:** 01 August 2022

Keywords: Canonical correlation coefficients; fail-safe; Fisher information matrix; redundancy; sensor placement optimization

Abstract



Sensor placement optimization (SPO) is usually applied during the structural health monitoring sensor system design process to collect effective data. However, the failure of a sensor may significantly affect the expected performance of the entire system. Therefore, it is necessary to study the optimal sensor placement considering the possibility of sensor failure. In this article, the research focusses on an SPO giving a fail-safe sensor distribution, whose sub-distributions still have good performance. The performance of the fail-safe sensor distribution with multiple sensors placed in the same position will also be studied. The adopted data sets include the mode shapes and corresponding labels of structural states from a series of tests on a glider wing. A genetic algorithm is used to search for sensor deployments, and the partial results are validated by an exhaustive search. Two types of optimization objectives are investigated, one for modal identification and the other for damage identification. The results show that the proposed fail-safe sensor optimization method is beneficial for balancing the system performance before and after sensor failure.

Impact Statement

The work in this article provides sensor placement optimization strategies bringing the possibility of sensor failure and backup sensors into consideration, for wired sensor systems. The focus is on optimization for modal identification or damage identification. The sensor deployments obtained can provide excellent performance when all sensors are working normally and guarantee good performance when partial sensors fail. Furthermore, it is shown that it is inadvisable to use backup sensors in wired sensor systems when the sensors are independent of each other.

1. Introduction

Sensor placement optimization (SPO) is a process of optimizing the number and location of sensors for a specific objective, to reduce instrument and processing costs without compromising the effect of monitoring. A statistical model is usually established to provide a quantitative objective function based on model parameters or the function of a model.

  This research article was awarded an Open Data and Open Materials badge for transparent practices. See the Data Availability Statement for details.

© The Author(s), 2022. Published by Cambridge University Press. This is an Open Access article, distributed under the terms of the Creative Commons Attribution licence (<http://creativecommons.org/licenses/by/4.0>), which permits unrestricted re-use, distribution and reproduction, provided the original article is properly cited.

According to the assumptions of model parameters, that is, whether a prior is placed on the parameters, the notions of objective functions can be divided into classical and Bayesian ones. Kammer (1991) and Yao et al. (1993) used a linear model to describe the relationship between sensor outputs and target mode shapes and optimized sensor combinations to maximize estimation quality of target modal coordinates. The difference between the classical optimization objectives adopted by Kammer (1991) and Yao et al. (1993) is the scalarization approach of the covariance of variable errors. Further studies of mode shape-based SPO, taking into account modeling errors and measurement noise, can be found in Kammer (1992a,b) and Jaya et al. (2020). Objective functions may use quantities in information theory, such as entropy and mutual information, or may use concepts from Bayesian statistics. Papadimitriou (2004) parameterized a structural model to describe the input–output behavior of a structure, and information entropy was used to measure uncertainty of the parameters updated by the measurements from a set of sensors. The sensor combination corresponding to the smallest entropy, in other words, the smallest uncertainty of the estimated parameters, was chosen as the optimal result. Krause et al. (2008) took a model used in spatial statistics—a Gaussian process—and used mutual information to measure the effect of selected sensors on the predictive uncertainty of variables in unobserved locations, so that the prediction quality over the whole space of interest was considered. In this case, the sensor combination corresponding to the largest mutual information, or rather to the maximum reduction in the uncertainty of responses from unobserved locations, was chosen as the optimal one.

When it comes to optimization objectives using a model function as the basis, most of them are related to supervised approaches, in which data for different structural states are involved to train a model. Worden and Burrows (2001) adopted an established supervised learning algorithm—a neural network—to rank a structural health monitoring (SHM) sensor layout according to the normalized mean-square error between the desired responses and estimated responses and probability of misclassification. The sensor deployment with the minimum weighted fitness value was treated as the optimal result. Considering the ability to classify a large amount of multivariate data, Eshghi et al. (2019) used a Mahalanobis distance classifier to carry out the reliability-based sensor system design to minimize the area of sensor patches while satisfying the detectability requirement for different health states. If a prior is placed on the probability of the potential outcomes of various structural states, the Bayes risk can be used as an objective function to minimize the cost of each outcome, which is demonstrated in Flynn and Todd (2010).

Some comprehensive references on SPO for SHM are available in Ostachowicz et al. (2019), Barthorpe and Worden (2020), and Tan and Zhang (2020) and Barthorpe and Worden (2020). Ostachowicz et al. (2019) discuss the optimisation objective functions corresponding to each SHM technique more systematically, by dividing the SHM techniques into three types. Tan and Zhang (2020) put more effort into classifying and comparing the optimisation algorithms, which are treated as consisting of five different types. In particular, the development of evolutionary optimisation methodologies and sequential sensor placement algorithms is clearly illustrated. Barthorpe and Worden (2020) provide a more complete demonstration of optimisation objectives and specify emerging trends and future directions of SHM SPO.

The scope of the current article belongs to the classical optimization criteria based on model parameters. However, except for the traditional objective functions based on mode shapes, a predefined criterion based on canonical correlations, originally developed by Hotelling (1936), is firstly used to evaluate a sensor layout, which can transfer the function of linear discriminant analysis into the parameter estimation issue (Sun and Chen, 2007). One reason for using this criterion is that it is usually more computationally efficient than criteria depending on model training. In existing research, correlation-based criteria have been widely applied in feature selection (Hall, 1999; Yu and Liu, 2003; Zhang and Lang, 2022), and some efforts have been made to extend its application to the SPO field. Chen et al. (2020) defined a coefficient to quantify the geometric correlation of probability distributions of data collected by pairs of sensors. Sensor pairs with larger correlation indexes were selected to provide the data for predicting the shapes of all probability density functions. However, the redundancy and interaction of information from different sensors were not considered in this article. Lu et al. (2016) narrowed the range

of sensor selection by maximizing the coefficient based on a correlation matrix and then minimized the correlation of the data provided by these candidate sensors to determine the final optimization result, but still ignored the information interaction. In contrast, the criteria based on canonical correlations can inherently take account of the information redundancy and interaction (Hall, 1999; Zhang and Lang, 2022), which is another reason for using this kind of criterion as an optimization objective in this article.

In addition, sensor failures may seriously affect the overall performance of the sensor system, especially when sensors that collect unique and critical information fail; therefore, it is necessary to study the optimization of sensor systems that consider the effects of sensor failures. For wired sensor networks, Side et al. (1997) developed a novel optimization idea for fail-safe sensor distributions. By maximizing the worst performance of $N - 1$ -sensor distributions generated by an N -sensor distribution, this optimization approach can provide a sensor set that can maintain an acceptable level of damage identification performance after a sensor failure. However, the objective function was only composed of the *child* fitness, which led to a conflict between the fail-safe *mother* distribution and optimal mother distribution. In this article, the improved fail-safe optimization method will be proposed to comprehensively consider the fitness of the mother distribution and worst sub-distribution for modal identification and damage identification.

For wireless sensor networks, Bhuiyan et al. (2013) proposed a backup or redundant sensor placement algorithm by incorporating the requirements of SHM and the limitations of wireless sensor networks to ensure a given level of fault tolerance. The case study showed that if the effects of sensor failures were not handled properly, it is meaningless to apply wireless sensor networks to SHM. Note that, for wireless sensor networks, sensor nodes within a sensor field will cooperate along designed routes through wireless connections, to transmit data to the base station; therefore, the failure of one sensor may affect the acquisition of data from other sensors. More information about wireless sensors and the wireless SPO can be found in Iqbal et al. (2015) and Abdollahzadeh and Navimipour (2016). Therefore, for the wireless sensor network, except the effects of sensor failures, solutions to deal with failures, such as placing backup sensors, must be considered during optimization, as demonstrated by Bhuiyan et al. (2013). This article assumes a wired sensor network where the failure of each sensor will not affect the data acquisition of other sensors and discusses whether it is worthwhile to design a sensor network with redundant sensors. Here, *sensor failure* refers to a situation where the sensor fails to provide any usable information, regardless of whether it is damaged or unable to connect to the network. Since the main task of this article is to evaluate whether the effects or the countermeasures of sensor failures need to be considered in the optimization process, how to evaluate whether the sensor is damaged is beyond the scope of this current article.

The major novelties of this article include:

1. This article studies the sensor location optimization algorithm considering sensor failure for both modal identification and damage identification. It is worth mentioning that the objective function for damage identification is based on canonical correlation analysis, which is the *first use* for SPO.
2. The optimization process of the fail-safe sensor distribution is improved. In addition to considering the performance of sensor distributions after sensor failure, the performance of the initial distribution is also integrated into the optimization process.
3. An optimization concept for the distribution of fail-safe redundant sensors is proposed. In the optimization design of the wired sensor deployment, the solution to deal with the failed sensor is considered, and then the value of this solution is discussed.
4. The approach is validated on a real structure, a full wing of a glider aircraft.

The article is organized as follows: the next section introduces the theoretical basis of the four optimization objectives belonging to two types of optimization purposes. Section 3 demonstrates the optimization flow to obtain fail-safe sensor distributions and fail-safe distributions with redundancy. Section 4 describes the tests on a glider wing to provide data for the case study. A series of results are presented and discussed in Section 5. The article is summarized at the end.

2. Optimization Objectives

The optimization objectives used for SPO depend on the purpose of the system and include the determinant of the Fisher information matrix (DFIM), the DFIM weighted by average-driving-point residue (DFIM-ADPR), the sum of squared canonical correlation coefficients (SSC), and the SSC weighted by average-driving-point residue (SSC-ADPR). The first two objectives, developed by Yao et al. (1993) and Imamovic and Ewins (1997), are widely used in SPO tasks, but the last two objectives are used for SPO for the first time. These objectives are selected or proposed from three perspectives, including the accuracy of the target modal-coordinate estimate, the vibration energy, and the information on the damage of interest. The detailed introduction is as follows.

2.1. Determinant of the Fisher information matrix

For the modal identification task, assume that there are limited candidate sensor locations and J modes to be identified. Suppose I sensors will be selected from the candidate sensors. The project budget determines the maximum value of I . For the s th combination of the I sensor locations, the outputs of these chosen sensors are described by a vector $\mathbf{y}_s \in \mathbb{R}^{I \times 1}$, which is given by,

$$\mathbf{y}_s = \mathbf{\Phi}_s \mathbf{q}_s + \varepsilon_s \tag{1}$$

where $\mathbf{\Phi}_s \in \mathbb{R}^{I \times J}$ is the s th target modal matrix, $\mathbf{q}_s \in \mathbb{R}^{J \times 1}$ is the vector of the target modal coordinates, and $\varepsilon_s \in \mathbb{R}^{I \times 1}$ is the vector of measurement noise at these selected sensors, which is assumed to be zero-mean Gaussian noise. The least-squares estimate of the target modal coordinates for the s th sensor combination can be acquired from,

$$\hat{\mathbf{q}}_s = (\mathbf{\Phi}_s^T \mathbf{\Phi}_s)^{-1} \mathbf{\Phi}_s^T \mathbf{y}_s \tag{2}$$

It can be seen that I should not be less than J to make $\mathbf{\Phi}_s$ invertible.

According to Beck and Arnold (1977), it can be assumed that the probability density function of $\hat{\mathbf{q}}_s$ is Gaussian, and the corresponding confidence region can be treated as the interior of the hyperellipsoid,

$$(\hat{\mathbf{q}}_s - \mathbf{q}_s)^T \mathbf{F}_{\hat{\mathbf{q}}_s}^{-1} (\hat{\mathbf{q}}_s - \mathbf{q}_s) = c^2 \tag{3}$$

where $\mathbf{F}_{\hat{\mathbf{q}}_s} = (\mathbf{\Phi}_s^T \mathbf{\Phi}_s)^{-1} \mathbf{\Phi}_s^T \mathbf{E}(\varepsilon_s \varepsilon_s^T) \mathbf{\Phi}_s (\mathbf{\Phi}_s^T \mathbf{\Phi}_s)^{-1}$ is the covariance matrix of the estimation error of $\hat{\mathbf{q}}_s$ and c is a constant related to the confidence level. The volume D_s of the hyperellipsoid can be obtained by Yao et al. (1993),

$$D_s = \pi^{I/2} c^I [\det(\mathbf{F}_{\hat{\mathbf{q}}_s})]^{1/2} [\Gamma(I/2 + 1)]^{-1} \tag{4}$$

where $\Gamma(\cdot)$ refers to the gamma function and $\det(\cdot)$ refers to the determinant. To obtain the best linear unbiased estimator, that is, the most accurate estimation of the target modal coordinates, the volume of this confidence region should be minimized. Because $\mathbf{F}_{\hat{\mathbf{q}}_s}$ is the only variable in Equation (4), the key to the optimization problem is to minimize the determinant of $\mathbf{F}_{\hat{\mathbf{q}}_s}$. As it was assumed that the measurement noise of sensors was uncorrelated and of equal variance σ^2 in Yao et al. (1993), they showed that,

$$\begin{aligned} \det(\mathbf{F}_{\hat{\mathbf{q}}_s}) &= \det[\sigma^2 (\mathbf{\Phi}_s^T \mathbf{\Phi}_s)^{-1}] \\ &= \sigma^{2I} \det[(\mathbf{\Phi}_s^T \mathbf{\Phi}_s)]^{-1} \end{aligned} \tag{5}$$

Because the $\mathbf{F}_{\hat{\mathbf{q}}_s}^{-1}$ was defined as the Fisher information matrix (FIM) in Middleton (1996), $\mathbf{\Phi}_s^T \mathbf{\Phi}_s$ was subsequently referred to as the FIM in Kammer (1991). Thus, minimizing the determinant of $\mathbf{F}_{\hat{\mathbf{q}}_s}$, as discussed earlier, is equivalent to maximizing the DFIM, that is, maximizing $\det(\mathbf{\Phi}_s^T \mathbf{\Phi}_s)$. Note that when the lower-upper (LU) decomposition is applied, the computational complexity of calculating the DFIM is $\mathcal{O}(J^3)$. Based on this, the FIM-based criterion can be applied to compare the different sensor combinations with the same number of sensors to find the optimal sensor deployment that is most beneficial to estimate the target modal coordinates most accurately.

2.2. DFIM average driving-point residue

There is an obvious disadvantage of using the DFIM as an optimization objective, in that sensor locations with low signal strength can be selected. In order to overcome this issue and improve the signal-to-noise ratio, the ADPR can be combined with the DFIM to give the $\det(\Phi_s^T \Phi_s)_{ADPR}$ corresponding to one sensor combination (Imamovic and Ewins, 1997), which is defined as,

$$\det(\Phi_s^T \Phi_s)_{ADPR} = \det(\Phi_s^T \Phi_s) \sum_{i=1}^I \sum_{j=1}^J \frac{(\phi_s^{ij})^2}{\omega_j} \tag{6}$$

where ϕ_s^{ij} is the entry corresponding to the i th degree of freedom of the j th target mode in the s th target modal matrix and ω_j is the natural frequency corresponding to the j th target mode. This criterion, the DFIM–ADPR, should be maximized to find the optimal sensor deployment.

2.3. Sum of squared canonical correlation coefficients

For the damage identification task, to make the sensor system have good performance in identifying certain damage states of concern, information about these high-potential failures should be included in the sensor system optimization process. These damage states can be determined by conducting failure mode analysis and referring to historical data about damage states collected on the existing structures.

The SSC is used here as a criterion to measure the maximal linear association between two co-occurring multivariate random variables with K observations, which are collected as matrices $\mathbf{X} \in \mathbb{R}^{K \times M}$ and $\mathbf{Y} \in \mathbb{R}^{K \times N}$ (Hotelling, 1936). In this article, a matrix \mathbf{X} represents the K samples of M features. A matrix \mathbf{Y} refers to labels represented by N variables associated with each sample. This criterion can help to directly measure the effectiveness of data for predicting structural states to a certain extent, without the need for model training. Furthermore, since a set of features in \mathbf{X} are evaluated together, rather than evaluating each feature individually, the interaction of features can be considered, avoiding redundant features.

The acquisition of the SSC can be realized by finding pairs of projection directions $\mathbf{U} \in \mathbb{R}^{M \times L}$ and $\mathbf{V} \in \mathbb{R}^{N \times L}$, so that the Pearson’s correlation coefficient between $\mathbf{X}_C \mathbf{u}_l$ and $\mathbf{Y}_C \mathbf{v}_l$ for the l th pair of projection directions is maximized (Zhang and Lang, 2022), that is,

$$\begin{aligned} R_l(\mathbf{X}, \mathbf{Y}) &\triangleq \max_{\mathbf{u}_l, \mathbf{v}_l} r(\mathbf{X} \mathbf{u}_l, \mathbf{Y} \mathbf{v}_l) \\ &\triangleq \max_{\mathbf{u}_l, \mathbf{v}_l} \frac{\mathbf{u}_l^T \mathbf{X}_C^T \mathbf{Y}_C \mathbf{v}_l}{\sqrt{\mathbf{u}_l^T \mathbf{X}_C^T \mathbf{X}_C \mathbf{u}_l} \sqrt{\mathbf{v}_l^T \mathbf{Y}_C^T \mathbf{Y}_C \mathbf{v}_l}} \end{aligned} \tag{7}$$

where $\mathbf{X}_C = \mathbf{X} - \bar{\mathbf{X}}$ and $\mathbf{Y}_C = \mathbf{Y} - \bar{\mathbf{Y}}$. $\bar{\mathbf{X}}$ and $\bar{\mathbf{Y}}$ are the means of columns of \mathbf{X} and \mathbf{Y} , respectively. $R(\cdot)$ refers to the canonical correlation coefficient and $r(\cdot)$ refers to the Pearson’s correlation coefficient. It can be seen that $R_l(\mathbf{X}, \mathbf{Y})$ does not depend on the scale of \mathbf{u}_l and \mathbf{v}_l . Therefore, the $\mathbf{X} \mathbf{u}_l$ and $\mathbf{Y} \mathbf{v}_l$ can be standardized to have unit variance. Then, Equation (7) can be expressed as,

$$\max_{\mathbf{u}_l, \mathbf{v}_l} \mathbf{u}_l^T \mathbf{X}_C^T \mathbf{Y}_C \mathbf{v}_l, \quad s.t. \mathbf{u}_l^T \mathbf{X}_C^T \mathbf{X}_C \mathbf{u}_l = 1, \mathbf{v}_l^T \mathbf{Y}_C^T \mathbf{Y}_C \mathbf{v}_l = 1 \tag{8}$$

Lagrange multipliers α and β can be used to find \mathbf{u}_l and \mathbf{v}_l , such that,

$$F(\mathbf{u}_l, \mathbf{v}_l) = \mathbf{u}_l^T \mathbf{X}_C^T \mathbf{Y}_C \mathbf{v}_l - \frac{1}{2} \alpha (\mathbf{u}_l^T \mathbf{X}_C^T \mathbf{X}_C \mathbf{u}_l - 1) - \frac{1}{2} \beta (\mathbf{v}_l^T \mathbf{Y}_C^T \mathbf{Y}_C \mathbf{v}_l - 1) \tag{9}$$

followed by,

$$\frac{d}{d\mathbf{u}_l} (F(\mathbf{u}_l, \mathbf{v}_l)) = \mathbf{X}_C^T \mathbf{Y}_C \mathbf{v}_l - \alpha \mathbf{X}_C^T \mathbf{X}_C \mathbf{u}_l = \mathbf{0} \tag{10}$$

$$\frac{d}{d\mathbf{v}_l} (F(\mathbf{u}_l, \mathbf{v}_l)) = \mathbf{X}_C^T \mathbf{Y}_C \mathbf{u}_l - \beta \mathbf{Y}_C^T \mathbf{Y}_C \mathbf{v}_l = \mathbf{0} \tag{11}$$

Premultiplying Equations (10) and (11) by \mathbf{u}_l^T and \mathbf{v}_l^T respectively, gives

$$\mathbf{u}_l^T \mathbf{X}_C^T \mathbf{Y}_C \mathbf{v}_l - \alpha \mathbf{u}_l^T \mathbf{X}_C^T \mathbf{X}_C \mathbf{u}_l = 0 \tag{12}$$

$$\mathbf{v}_l^T \mathbf{X}_C^T \mathbf{Y}_C \mathbf{u}_l - \beta \mathbf{v}_l^T \mathbf{Y}_C^T \mathbf{Y}_C \mathbf{v}_l = 0 \tag{13}$$

It can be found that $R_l(\mathbf{X}, \mathbf{Y}) = \alpha = \beta$.

By a series of transformations based on Equations (10) and (11), the values of $R(\mathbf{X}, \mathbf{Y})$ can be obtained by solving the eigenvalue equations given by Hardoon et al. (2004) and Cox (2005),

$$\left[(\mathbf{X}_C^T \mathbf{X}_C)^{-1} \mathbf{X}_C^T \mathbf{Y}_C (\mathbf{Y}_C^T \mathbf{Y}_C)^{-1} \mathbf{Y}_C^T \mathbf{X}_C - R_l^2(\mathbf{X}, \mathbf{Y}) \mathbf{I} \right] \mathbf{u}_l = 0 \tag{14a}$$

$$\left[(\mathbf{Y}_C^T \mathbf{Y}_C)^{-1} \mathbf{Y}_C^T \mathbf{X}_C (\mathbf{X}_C^T \mathbf{X}_C)^{-1} \mathbf{X}_C^T \mathbf{Y}_C - R_l^2(\mathbf{X}, \mathbf{Y}) \mathbf{I} \right] \mathbf{v}_l = 0 \tag{14b}$$

The corresponding projection directions $\mathbf{u}_l \in \mathbb{R}^{M \times 1}$ and $\mathbf{v}_l \in \mathbb{R}^{N \times 1}$ are also obtained now. Since $R_l(\mathbf{X}, \mathbf{Y})$ ranges between -1 and 1 , the eigenvalue $R_l^2(\mathbf{X}, \mathbf{Y})$ takes values between 0 and 1 . If \mathbf{X}_C and \mathbf{Y}_C have full column rank, the number of the non-zero eigenvalues is not greater than $\min(M, N)$, that is, L is not greater than $\min(M, N)$.

On this basis, the sum of non-zero eigenvalues, that is, SSC, is adopted as a criterion for evaluating the effectiveness of a feature set from a sensor set to infer the structural state, which is given by,

$$\begin{aligned} \sum_{l=1}^L R_l^2(\mathbf{X}, \mathbf{Y}) &= \text{tr} \left[(\mathbf{X}_C^T \mathbf{X}_C)^{-1} \mathbf{X}_C^T \mathbf{Y}_C (\mathbf{Y}_C^T \mathbf{Y}_C)^{-1} \mathbf{Y}_C^T \mathbf{X}_C \right] \\ &= \text{tr} \left[(\mathbf{Y}_C^T \mathbf{Y}_C)^{-1} \mathbf{Y}_C^T \mathbf{X}_C (\mathbf{X}_C^T \mathbf{X}_C)^{-1} \mathbf{X}_C^T \mathbf{Y}_C \right] \end{aligned} \tag{15}$$

where $\text{tr}[\cdot]$ represents the trace of a matrix. The computational complexity of Equation (15) is $\mathcal{O}(M^2K)$ when $N \leq M$ or $\mathcal{O}(N^2K)$ when $N > M$. According to the SSC criterion, the optimal sensor deployment with the largest SSC among sensor combinations with the same number of sensors is conducive to the most accurate estimation of the structural labels because the features are more correlated with labels.

2.4. SSC average driving-point residue

If mode shapes are used as features for SPO with the aim of damage identification, the selected n mode shapes collected under different structural states can form a feature matrix $\mathbf{X}_s \in \mathbb{R}^{K \times (I \times J)}$ corresponding to the s th combination of I sensors. Rows refer to K observations for different healthy states, and columns refer to the relative displacement of I selected sensor locations on a structure in J modes. What is worth noting is that if only one mode shape is going to be considered, that is, $J = 1$, the feature corresponding to i th sensor location will be a vector $\mathbf{x}_s^i \in \mathbb{R}^{K \times 1}$; if more than one mode shape is considered, that is, $J > 1$, the feature corresponding to i th sensor location will be a matrix $\mathbf{X}_s^i \in \mathbb{R}^{K \times J}$.

Similarly, the ADPR coefficient can be combined with SSC to improve the stability of the optimal sensor layout to noise, which is given by,

$$\sum_{l=1}^L R_l^2(\mathbf{X}, \mathbf{Y})_{\text{ADPR}} = \sum_{l=1}^L R_l^2(\mathbf{X}, \mathbf{Y}) \sum_{k=1}^K \sum_{i=1}^I \sum_{j=1}^J \frac{(x_s^{kij})^2}{\omega_j^k} \tag{16}$$

where x_s^{kij} is the entry corresponding to the i th degree of freedom of the j th target mode from the k th observation of the s th target modal matrix and ω_j^k is the natural frequency corresponding to the j th target mode in the k th observation. When the number of sensors is fixed, the sensor deployment with the largest SSC-ADPR will be considered the optimal sensor placement.

2.5. Discussion and handling of singular matrices

From Equations (5), (6), (15) and (16), it can be seen that these four optimization objectives are not applicable for the SPO with singular matrices, including the mode shape matrix (Φ), the feature matrix (X), and the label matrix (Y), which are not invertible. This means that it is necessary to check whether these matrices are singular before optimization using these four objectives.

Since the mode shapes are independent when the number of degrees of freedom is equal to or greater than the number of identified modes and the selected degrees of freedom are not centrally distributed, the singularity problem for a mode shape matrix (Φ) can be solved by increasing the candidate sensor locations and changing the distribution of the candidate sensor locations. For the feature matrix (X), the sensor combination corresponding to a singular feature matrix can be discarded directly. Usually, the label matrix (Y) is of full rank. If not, the redundant label information should be removed first.

3. Optimization Considering Sensor Failure and Sensor Redundancy

In order to make the performance of the sensor system less sensitive to sensor failures, two novel optimization ideas are proposed by combining the above optimization objectives with the effects of, or countermeasures to, sensor failures to obtain the fitness of sensor distribution.

The first approach, called the *fail-safe sensor distribution*, will take into account the effects of critical sensor failures when calculating the fitness of the sensor distribution. The second approach is called the *fail-safe sensor distribution with redundancy*, where the fitness results of the sensor distribution will be affected by the key critical failure handling scheme. The motivation for the second optimization idea is to explore, with a fixed number of sensors, a better strategy to place all sensors in different locations, to collect more information, or use a subset of sensors as backup sensors for key sensors. The evaluation criterion is based on the performance of the sensor system before and after the failure of the key sensor.

To make the formulation of these two optimization strategies more explicit in the following sections, SPO is framed here as a combinatorial optimization problem. This article does not address the case of describing sensor locations in continuous space. The number of combinations S for selecting I sensors from Z candidate sensors in different locations is given by,

$$S = {}_Z C_I = \frac{Z!}{I!(Z-I)!} \quad (17)$$

3.1. Fail-safe sensor optimization

The process of SPO with sensor failures under consideration can be divided into two stages. At the first stage, the “fail-safe” fitness of an algorithm is defined and obtained by taking the worst fitness value of the $(I - I_F)$ -sensor distributions generated from an I -sensor distribution by removing I_F sensors. I_F refers to the number of sensors that are allowed to fail without requiring any remedial action. Note that the I -sensor distribution refers to the I sensors being put in I different locations. Because $(I - I_F)$ sensor locations will be selected from the mother distribution of I sensor locations, the number of combinations S_{FS} for the fail-safe fitness is

$$S_{FS} = S \cdot {}_I C_{(I-I_F)} = S \cdot I C_{I_F} = \frac{Z!}{I_F!(Z-I)!(I-I_F)!} \quad (18)$$

Note that ${}_I C_{(I-I_F)}$ equals $I C_{I_F}$, because the number of all child distributions containing functioning sensors is equal to the number of all combinations with failed sensors. For the sake of brevity, the more concise expression, $I C_{I_F}$, will be used below. Then, the maximum/minimum fail-safe fitness values are going to specify the optimal fail-safe sensor distribution.

The first stage here provides a more general description of the fail-safe sensor distribution idea introduced in Side et al. (1997). However, there may be multiple optimal combinations where sub-distributions corresponding to the worst fitness are the same. Nonetheless, the search algorithm will provide only one of these optimal I -sensor combinations of different fitness, but the same fail-safe fitness.

Therefore, after obtaining an optimal fail-safe sensor distribution given by a search algorithm, at the second stage, the following steps should be taken to further consider the performance of the I -sensor distribution:

1. Replace the sensors for which failures lead to the worst performance, with other candidate sensors from the $Z - I$ unselected sensors. The number of updated I -sensor distributions is

$$S_{UPD} = {}_{(Z-I)}C_{I_F} = \frac{(Z - I)!}{I_F!(Z - I - I_F)!} \tag{19}$$

2. Calculate the performance of the $(I - I_F)$ -sensor distributions generated by the updated I -sensor distribution. The number of the child distributions for these updated mother distributions is given by,

$$S_{UPDFS} = S_{UPD} \cdot I C_{I_F} = \frac{I!(Z - I)!}{(I_F!)^2(Z - I - I_F)!(I - I_F)!} \tag{20}$$

Compare the worst fitness value of these $(I - I_F)$ -sensor distributions with the corresponding fail-safe fitness result of the optimal sensor layout found at the first stage. Retain the sensor distribution if both fitness values are the same.

3. Calculate the performance of all such retained I -sensor distributions and the optimal sensor distribution obtained at the first stage. Select the sensor distribution with the largest fitness value as the final optimal fail-safe sensor distribution, which is named the optimal improved-fail-safe sensor distribution.

An example is given in Section 5.1 to show all the steps of the fail-safe optimization strategy. Note that the three steps in the second stage are not the most efficient way to find the optimal fail-safe sensor distribution with the largest fitness value for an exhaustive search (ES). Multiple optimal fail-safe combinations can be directly found by filtering out the combinations with the best fail-safe fitness. However, the three steps described above are applicable when not all candidate solutions are available.

3.2. Fail-safe sensor optimization with redundancy

To further improve the performance of the sensor system after any sensor fails, compared with putting I sensors in I different locations, I_F of the I sensors can be used as redundant sensors and be added to I_F critical locations of the $I - I_F$ sensor locations. This idea can help to avoid the worst performance of the $[(I - I_F) - I_F]$ -sensor distributions generated by an $(I - I_F)$ -sensor distribution without increasing the number of sensors used. Based on this, the fail-safe SPO with sensor backup under consideration can also be divided into two stages.

At the first stage, $I - I_F$ locations will be selected first from the Z candidate locations. The maximum/minimum fail-safe fitness value is going to be reached to find the optimal fail-safe sensor distribution with $I - I_F$ sensors. Backup sensors are then added to the locations of the I_F key sensors, to avoid the occurrence of the $[(I - I_F) - I_F]$ -sensor distributions with the worst performance. The “fail-safe with redundancy” fitness is then defined and obtained by taking the worst fitness value of the $(I - I_F)$ -sensor distributions with redundancy, generated from an I -sensor distribution with redundancy by omitting I_F “non-critical” sensors (sensors without a backup sensor) in turn. Note that the I -sensor distribution with redundancy means that I sensors are placed in $I - I_F$ different locations, with I_F pairs of sensors in the same location. The number of combinations S_{FSR} , for the fail-safe with redundancy fitness is

$$S_{\text{FSR}} = z C_{(I-I_F)^{(I-I_F)} C_{I_F}^{[(I-I_F)-I_F]} C_{I_F} = \frac{Z!}{(I_F!)^2 (Z-I+I_F)! (I-3I_F)!} \quad (21)$$

The maximum/minimum fail-safe with redundancy fitness value is then going to specify the optimal I -sensor distribution with redundancy. Furthermore, it is necessary to clarify that the intended function of redundant sensors (or backup sensors) is to provide the same information when some of the original sensors cease to provide valid information. Therefore, the existence of the redundant sensors is to avoid the worst-case scenario, after the failure of the key sensors. Data from redundant sensors are not used when computing the fail-safe with redundancy fitness. On this basis, optimal results for the fail-safe SPO with redundancy can be obtained.

Similarly, more than one optimal fail-safe sensor distribution with redundancy may be included for the case with the same number of selected sensors. Considering the performance of these sensor distributions before any sensor fails, the sensor distribution with the greatest fitness should be chosen as the final optimal fail-safe sensor distribution with redundancy. Therefore, after obtaining the optimal fail-safe sensor distributions with redundancy at the first stage, the results should be evaluated and updated via the following steps at the second stage:

1. Replace the I_F sensors whose failure corresponds to the optimal fail-safe with redundancy fitness with other candidate sensors from the $Z - (I - I_F)$ unselected sensors.
2. Compare the worst fitness value of the $(I - I_F)$ -sensor distributions with redundancy, generated by omitting I_F “non-critical” sensors in turn, with the corresponding fail-safe with redundancy fitness result of the optimal sensor deployment found at the first stage. And retain the I -sensor distribution with redundancy if the two fitness values are the same. The number of the child distributions with redundant sensors for the updated mother distributions with redundant sensors is

$$S_{\text{UPDFSR}} = [Z-(I-I_F)] C_{I_F}^{[(I-I_F)-I_F]} C_{I_F} = \frac{(I-2I_F)!(Z-I+I_F)!}{(I_F!)^2 (Z-I)! (I-3I_F)!} \quad (22)$$

3. Calculate the performance of all retained I -sensor distributions with redundancy and the optimal I -sensor distribution with redundancy obtained at the first stage. Select the sensor distribution with the largest fitness value as the final optimal fail-safe sensor distribution with redundancy, which is called the optimal improved-fail-safe sensor distribution with redundancy.

Section 5.2 gives an example of fail-safe sensor optimization with redundancy that includes all the steps above. Again, the three steps introduced here are not the most efficient way to find the best results for an ES, but they are more versatile given the different search algorithms.

3.3. Discussion and suggestions on the application of fail-safe strategies

The initial motivation for considering sensor failures in the sensor optimization process is that when one or two sensors fail, the performance of the sensor system remains within acceptable limits and no maintenance is required. Such sensor systems can be of value in situations where maintenance is difficult or expensive. When many sensors are not providing data properly, this is a very suspicious situation that needs to be detected by the maintenance team. So it does not make much engineering sense to design for the failure of many sensors. Moreover, it must be clarified that the fail-safe strategies here can only consider the worst-case scenario after sensor failure. However, since the worst case corresponds to the failure of several critical sensors, the loss of a smaller number of critical or non-critical sensors should correspond to better system performance than the worst case.

Furthermore, the idea of fail-safe is unnecessary when the budget for sensors and the corresponding data storage and processing is large enough to design a densely distributed sensor system, which means no sensor in this system is critical or irreplaceable. That is, in that sensor system, each sensor has at least one “backup” sensor to provide similar information. However, the fail-safe strategies in this article aim to

consider the impact of the failure of certain critical sensors in the optimization process of a sensor system and whether it is worthwhile to pre-place a backup sensor for critical sensors. Therefore, it should only be applied when designing a sensor system which includes critical sensors.

When all the degrees of freedom of the finite element model are used as candidate sensor positions, engineering experience can be used to reduce the density of candidate sensor distribution preliminarily. For example, sensors are evenly distributed to cover the area to be detected, and nodes with larger signal amplitudes are selected. In addition, a more objective criterion can be used to avoid arranging the sensors at adjacent locations where substantially the same information will be collected. For example, the linear correlation of features can also be used to determine whether a feature contains some uncorrelated information from the selected ones.

4. Illustrative Examples

A series of tests were performed on a glider wing in an environmental chamber (shown in Figure 1) to provide a data set suitable for this research.

4.1. Experiment setups

Thirty-six candidate sensor locations are available as shown in Figure 2, which is not drawn to scale. The damage of interest was simulated by adding a mass block (60 g) onto the structure. As demonstrated in Figure 2, three damage cases were considered: mass addition at locations [M1], [M2], and [M3].

A Gaussian white-noise excitation was generated and applied to the wing at a point between sensor 22 and sensor 23 using an ETS solutions VT100 electrodynamic shaker. Frequency response functions (FRFs) were measured using PCB resonant piezoelectric accelerometers (Model 353B18). These accelerometers are uniaxial and measure perpendicular to the surface on which they are mounted. The weight of each sensor is 1.8 gm. The measurement frequency range was 0–4,096 Hz with frequency resolution 0.25 Hz.

Three temperatures were controlled and recorded: 5, 10, 15°C. Only one measurement of the FRF matrix was recorded for the structure under the normal condition and each damaged condition at each controlled temperature. Each FRF is an averaged value of 20 measurements to make the obtained FRFs smoother. For more details on the experimental setups, please refer to Wang et al. (2021). Note that the simulated damage cases in that article are different from those in this article.

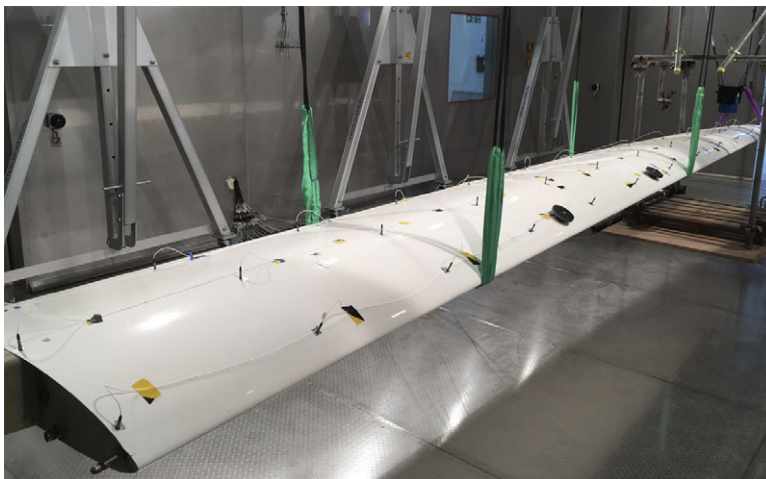


Figure 1. Photograph of the experiment setting in the testing chamber.

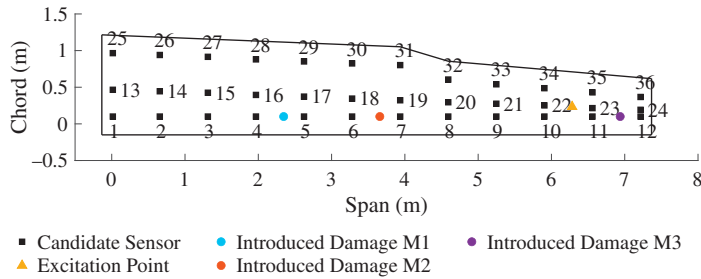


Figure 2. Labeled positions of significant points on the glider wing.

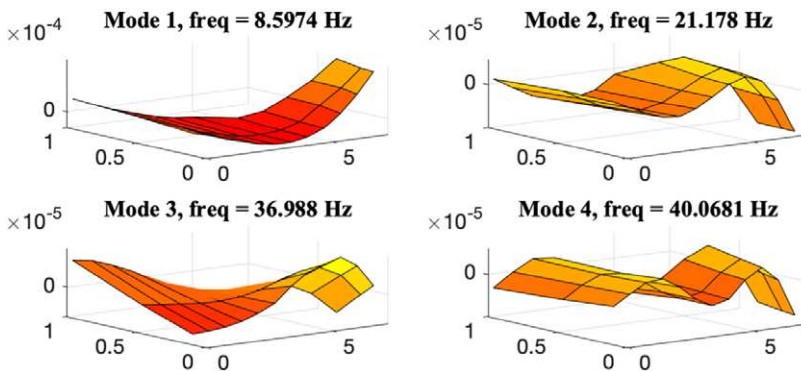


Figure 3. The first four mode shapes of the glider wing.

4.2. Data set for the SPO on modal identification

The first four mode shapes, denoted as Mode 1–4, and corresponding natural frequencies were extracted from the high-averaged FRFs, as shown in Figure 3.

For SPO with the aim of modal identification, three mode shapes of the wing under the normal condition at 15°C were chosen to form the s th target mode matrix $\Phi_s \in \mathbb{R}^{I \times 3}$ for the s th combination of the I sensor locations, including the first, second, and fourth mode shapes. The reason to adopt these three mode shapes is that by comparing the optimization results obtained by the two proposed fail-safe methods using the first three mode shapes and the selected three mode shapes separately, optimization results corresponding to the selected three mode shapes include more possible scenarios. Moreover, according to Equation (2), at least three sensors must be selected to provide a target modal matrix with full column rank, which means that the mode shapes are linearly independent (Yao et al., 1993).

4.3. Data set for the SPO on damage identification

For SPO with the aim of damage identification, mode shapes of the glider wing under four different health states with corresponding labels were used to form the feature matrix and the label matrix. For each mode shape, only one measurement is available for the structure in each health state at each controlled temperature. Thus, the available number of the observations K is the number of health states times the number of controlled temperatures, which is equal to 4×3 . This means that the number of columns ($I \times J$) in the feature matrix should not exceed $K = 12$ to form a full column rank feature matrix. Note that mode shapes for three temperatures are adopted here because mode shapes extracted from FRFs (if there are more than one) measured at one temperature may constitute a rank-deficient feature matrix \mathbf{X}_C . $\mathbf{X}_C^T \mathbf{X}_C$ will then be a singular matrix, which cannot be used for the SSC calculation.

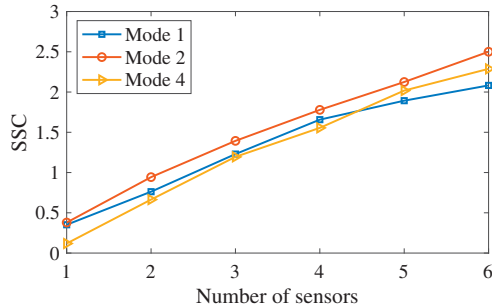


Figure 4. Comparison of ES results based on the SSC for three selected mode shapes.

Therefore, to allow more sensors to be selected to show the possible situation of optimization results as comprehensively as possible, each of the three mode shapes used in the SPO for modal identification was adapted to form the feature matrix $\mathbf{X}_s \in \mathbb{R}^{12 \times I}$ corresponding to the s^{th} combination of I sensors separately. Meanwhile, because the labels here are nominal data without an inherent order, four categorical variables are encoded into a matrix by dummy coding, which uses N features to represent $N + 1$ labels/categories. Therefore, the size of the label matrix is 12×3 . One reason for using dummy encoding is that it can make the label matrix \mathbf{Y} remain full column rank after subtracting its column mean.

For each mode shape, the SSC between the feature matrix and the label matrix of the structural state is calculated for sensor distributions with different numbers of sensors. An ES is used to find the optimal sensor combinations with one to six sensors for three mode shapes separately. The comparison of optimal fitness values for three selected mode shapes is presented in Figure 4. Because the SSC corresponding to the second mode shape (Mode 2) is always greater than that of others, this mode shape will be used to provide features to illustrate the proposed SPO ideas for damage identification.

The ADPR values calculated from the above two data sets were scaled so that their range is within the interval $[0,1]$, reducing the software's precision requirements for numeric calculations of objective functions involving the signal strength.

4.4. Optimization algorithms

Two optimization algorithms are chosen here to show the whole optimization process specifically: a deterministic algorithm—an ES, and a stochastic algorithm—a genetic algorithm (GA). Because of limitations in computer performance, a GA is mainly used to realize the search tasks. Results from the ES will be used for validation. It is necessary to say that the number of mother combinations presented in Section 3 is based on an ES. Finding the optimal result with a GA usually requires evaluating far fewer combinations of the mother distribution. In the search process of the two algorithms, the combination process of obtaining child distributions of a mother distribution is the same.

The parameters used for the GA are as follows: population size is 50, probability of crossover is 0.8, and probability of mutation is 0.01. The number of elite surviving to the next generation equals $0.05 \times$ population size (round toward positive infinity to the nearest integer). Linear fitness scaling is used. The algorithm stops when the average relative change in the fitness function is less than or equal to a tolerance. Considering the randomness of the initial population for the GA, it was run 10 times for each case, and the best among the 10 results was chosen as the final optimization result. For more information on GA and how to choose or optimize the parameters for GA, please refer to Eiben and Smith (2015).

An ES technique and a GA are first used to search for the optimal sensor distribution without considering sensor failure. The comparison of these two results can help to check the effectiveness of the GA. Furthermore, these two sets of results can be compared with the following results that consider sensor failure aspects, which are designed to be searched out via a GA. Part of the results corresponding to

a small number of sensors has also been searched exhaustively to verify the effectiveness of the GA application.

Note that considering the scalability of the algorithm, an evolutionary algorithm is suggested to be used, because it still be applicable when the number of candidate sensor combinations is very large. However, the reliability of optimal results will be an issue since evolutionary algorithms, such as the GA, may provide poor suboptimal results. In order to address this concern, a compromise solution is given here. A greedy algorithm can be used to search for suboptimal results, which can often be obtained in much less time than an ES. The GA results are then compared to the greedy search results to ensure that the GA results are at least as good as the greedy search results.

5. Results and Discussion

To more intuitively demonstrate the two ideas introduced in Section 3, take $I_F = 1$ as an example, which means that the number of sensors assumed to have failed in the design process is one. The number of backup sensors then corresponding to the key sensors is also one. It is then easy to find that the sub-distribution with the worst fail-safe with redundancy fitness should typically be obtained by performing the combination $[(I-I_F)-I_F]C_{I_F}$ in Equation (21). However, for the case of $I_F = 1$, these sub-distributions of sensors are the child distributions corresponding to the second-worst fail-safe fitness in the last step, which helps simplify the code.

At the risk of duplication, it should be stated that the fitness based on any of the four optimization objectives presented in Section 2 needs to be maximized to obtain the optimal sensor distribution.

5.1. Optimization results of improved fail-safe SPO

Firstly, the SPO based on DFIM is used to demonstrate the two-stage process of obtaining the optimal improved fail-safe sensor distribution. At the first stage, optimal fail-safe sensor distributions with four and five sensors are found by an ES and listed in Table 1. The optimization results for this type with four to eight sensors corresponding to a GA are given in Table 2.

The reasons for choosing the number of sensors to be four to eight are as follows. The minimum number of selected sensors depends on the number required to obtain valid fitness values for all four

Table 1. Optimal fail-safe sensor distributions obtained by an ES combined with the DFIM.

No. of sensors	Sensor number	Fail-safe fitness
4	4,12 ^a ,33,35	6.169e-08
5	4,12,31,34,36	3.182e-07
6	12,16,24,28,34,35	1.147e-06

Abbreviations: DFIM, determinant of the Fisher information matrix; ES, exhaustive search.

^aThe failure of a sensor at the position marked in blue will result in the worst fail-safe fitness.

Table 2. Optimal fail-safe sensor distributions obtained by an GA combined with the DFIM.

No. of sensors	Sensor number	Fail-safe fitness
4	4,12,33,35	6.169e-08
5	5,12,31,34,36	3.182e-07
6	12,16,24,28,34,35	1.147e-06
7	12,16,22,24,28,31,34	1.980e-06
8	12,16,22,24,28,31,34,36	3.334e-06

Abbreviations: DFIM, determinant of the Fisher information matrix; GA, genetic algorithm.

optimization objectives. When it comes to selecting the maximum number of sensors, it needs to be said that, considering the reliability of the conclusions obtained, the findings of this article will be based on the analysis of the results of the deterministic search algorithm. Therefore, the computational cost limits the maximum number of selected sensors by an ES to six. The optimal sensor distributions with seven and eight sensors obtained by the GA were used to verify the applicability of the findings obtained from the optimal sensor distributions of four to six sensors.

The design of up to eight sensors was selected from the 36 sensors, indicating that this illustrative example considers the case where the sensors are not densely arranged on the structure, which enables each sensor to collect mutually non-redundant information to a certain extent. In practice, the sensors are generally not arranged in a large number on a simple structure or a part of a complex structure considering data transmission, storage, and processing. However, this approach can be used to optimize systems with densely distributed sensors to account for the failure of some key sensors that collect critical information.

From Tables 1 and 2, it can be seen that the sensor distributions with five sensors obtained by the GA and the ES are a little different. However, by checking the fail-safe fitness values of these two distributions, the result turns to be the same. This result means that when the number of selected sensors is the same, multiple optimal fail-safe sensor distributions with the same fail-safe fitness value can be obtained. In this case, the fitness values of the mother distributions of these optimal fail-safe sensor distributions can be used to evaluate their performance and rank them.

At the second stage, considering the performance of these optimal fail-safe sensor distributions before any sensor fails, the sensor distribution with the largest DFIM should be selected as the final optimal fail-safe sensor distribution. Therefore, after obtaining the optimal fail-safe sensor distributions given by an ES or a GA at the first stage, these results should be evaluated and updated following the steps in Section 3.1. The situation of all optimal fail-safe distributions with four to eight sensors generated by the GA results is given in Table 3, and the optimal improved-fail-safe distributions with four to eight sensors are listed in Table 4. By comparing the fitness values of multiple optimal fail-safe sensor distributions for four, five, and seven sensors in Table 3, it can be seen that an improved fail-safe approach can bring some benefits without increasing the cost of sensing equipment.

The same process dependent on an ES and a GA is repeated to search for the optimal improved fail-safe sensor distributions corresponding to the other three optimization objectives—DFIM-ADPR, SSC, and SSC-ADPR, and the results of the GA are listed in Tables 8–10 in Supplementary Material S1.

Table 3. Multiple optimal fail-safe sensor distributions corresponding to the DFIM.

No. of sensors	Sensor number	Fail-safe fitness	Fitness
4	4,12,33,35	6.169e-08	4.923e-07
	4,24,33,35	6.169e-08	4.851e-07
	4,33,35,36	6.169e-08	4.840e-07
5	4,12,31,34,36	3.182e-07	1.408e-06
	5,12,31,34,36	3.182e-07	1.284e-06
	12,13,31,34,36	3.182e-07	1.073e-06
	12,16,31,34,36	3.182e-07	1.479e-06
	12,17,31,34,36	3.182e-07	1.234e-06
	12,25,31,34,36	3.182e-07	1.107e-06
	12,28,31,34,36	3.182e-07	1.621e-06
	12,29,31,34,36	3.182e-07	1.151e-06
	12,16,24,28,34,35	1.147e-06	2.783e-06
7	12,16,22,28,31,34,24	1.980e-06	3.940e-06
	12,16,22,28,31,34,36	1.980e-06	4.140e-06
	12,16,22,28,31,34,36	3.334e-06	6.128e-06

Abbreviation: DFIM, determinant of the Fisher information matrix.

Table 4. Optimal improved-fail-safe sensor distributions obtained by a GA combined with the DFIM.

No. of sensors	Sensor number	Fail-safe fitness	Fitness
4	4,12 ^a ,33,35	6.169e-08	4.923e-07
5	12,28,31,34,36	3.182e-07	1.621e-06
6	12,16,24,28,34,35	1.147e-06	2.783e-06
7	12,16,22,28,31,34,36	1.980e-06	4.140e-06
8	12,16,22,24,28,31,34,36	3.334e-06	6.128e-06

Abbreviations: DFIM, determinant of the Fisher information matrix; GA, genetic algorithm.

^aFrom a fail-safe perspective, the replaceable sensor location is marked in magenta.

Table 5. Optimal fail-safe sensor distributions with redundancy obtained by a GA combined with the DFIM.

No. of sensors	Sensor number	Fail-safe fitness
5	13 ^b ,31,34,36 (36) ^a	1.631e-07
6	12,16,28,34 (34),36	7.242e-07
7	4,12,16,34 (34),35,36	1.306e-06
8	4,12,16,24,28,34 (34),36	2.147e-06

Abbreviations: DFIM, determinant of the Fisher information matrix; GA, genetic algorithm.

^aSensors in parentheses are redundant sensors placed to avoid the worst fail-safe fitness.

^bThe failure of a sensor at the position marked in green will result in the worst fail-safe with redundancy fitness.

5.2. Optimization results of improved fail-safe with redundancy SPO

The two-stage process of the improved-fail-safe SPO with redundancy is illustrated using an objective function of a GA based on DFIM. At the first stage, the optimization results of the fail-safe sensor distributions with redundancy obtained by a GA are shown in Table 5. As before, more than one optimal result is included for the case with the same number of selected sensor locations, which is shown in Table 6. Considering the performance of these sensor distributions before any sensor fails, the sensor distribution with the largest DFIM should be selected as the optimal improved-fail-safe sensor distribution with redundancy. Therefore, after obtaining the optimal fail-safe sensor distributions with redundancy

Table 6. Multiple optimal fail-safe sensor distributions with redundancy corresponding to the DFIM.

No. of sensors	Sensor number	Fail-safe fitness	Fitness
5	4,31,34,36 (36)	1.631e-07	7.274e-07
	5,31,34,36 (36)	1.631e-07	6.619e-07
	13,31,34,36 (36)	1.631e-07	5.535e-07
	16,31,34,36 (36)	1.631e-07	7.623e-07
	17,31,34,36 (36)	1.631e-07	6.351e-07
	28,31,34,36 (36)	1.631e-07	8.333e-07
	29,31,34,36 (36)	1.631e-07	5.908e-07
	12,16,28,34 (34),36	7.242e-07	1.587e-06
6	4,12,16,34 (34),35,36	1.306e-06	2.614e-06
	4,12,28,34 (34),35,36	1.306e-06	2.822e-06
7	4,12,28,34 (34),35,36	1.306e-06	2.822e-06
8	4,12,28,34 (34),35,36	2.147e-06	3.432e-06

Abbreviation: DFIM, determinant of the Fisher information matrix.

Table 7. Optimal improved-fail-safe sensor distributions with redundancy obtained by a GA combined with the DFIM.

No. of sensors	Sensor number	Fail-safe fitness	Fitness
5	28,31,34,36 (36)	1.631e-07	8.333e-07
6	12,16,28,34 (34),36	7.242e-07	1.587e-06
7	4,12,28,34 (34),35,36	1.306e-06	2.822e-06
8	4,12,16,24,28,34 (34),36	2.147e-06	3.432e-06

Abbreviations: DFIM, determinant of the Fisher information matrix; GA, genetic algorithm.

given by a GA, these results should be evaluated and updated following the steps in Section 3.2 and the improved optimization results are shown in Table 7.

For other optimization objectives, including the DFIM-ADPR, the SSC, and the SSC-ADPR, the results of the optimal improved-fail-safe sensor distributions with redundancy obtained by a GA are shown in Tables 11–13 in Supplementary Material S2.

Similar to Section 5.1, a small number of sensors were selected in this part. However, this approach can also be used in situations where a large number of sensors need to be placed. This may cause some sensors to be brought close together to collect almost the same information. So the question becomes one of, how to find the optimal redundant sensor positions when the available sensor positions are limited and the number of sensors is greater than the sensor positions. In this case, the fail-safe SPO with redundancy in this article can be used as an alternative method to optimize redundant sensor placements.

5.3. Performance evaluation

In this part, three aspects will be discussed: the effectiveness of the GA algorithm, the performance of the sensor distributions obtained by the fail-safe SPO, and those obtained by the fail-safe with redundancy SPO.

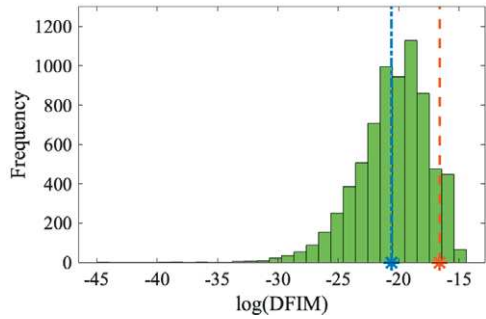
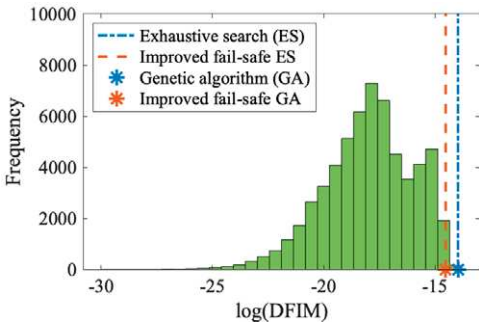
To better accomplish these tasks, except for the optimal sensor distributions considering sensor failure, the optimal sensor distributions only taking account of the fitness of mother distributions are found via ES and GA optimization strategies. This kind of SPO strategy is called “classical” SPO here. Four optimization objectives, DFIM, DFIM-ADPR, SSC, and SSC-ADPR are all involved. Moreover, in the case of a certain number of sensors, to compare the results of the three SPO strategies more intuitively, the results of the classical SPO, the fail-safe SPO, and the fail-safe with redundancy SPO corresponding to four optimization objectives are plotted in blue, orange, and yellow in Figures 5–8 separately.

Before comparing the optimal results obtained by the two applied search algorithms, it should be noted that: (a) when comparing the optimal results corresponding to an ES and a GA obtained by classical SPO (marked with a blue dash-dotted line and a blue asterisk, respectively), the fitness value before the sensor failure should be used, as shown in the left sub-figures and marked in blue. This choice is because, for classical SPO, the sensor deployment is optimized according to the fitness of the mother distribution. (b) For the optimal results obtained by the other two optimization strategies, it is necessary to compare the optimal fitness values corresponding to two search algorithms after the failure of the marked sensor, as shown in the right sub-figures and marked with orange or yellow dash-dotted lines and asterisks, because, for these two SPO, the sensor deployment is optimized on the worst child fitness.

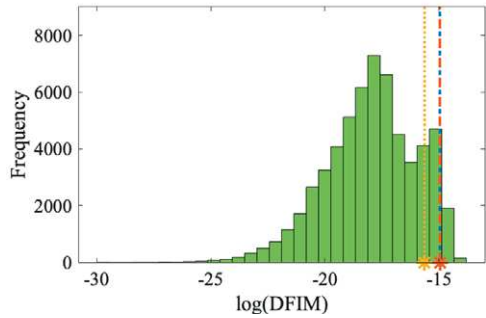
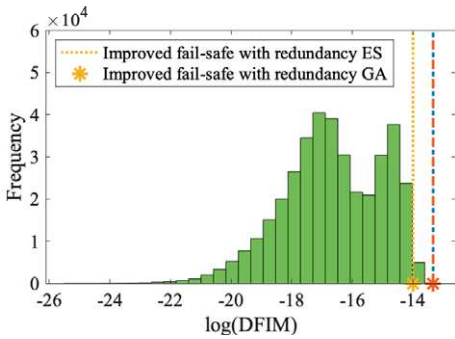
It can be seen that the optimal sensor deployments with three to five sensors obtained by the ES and the GA are the same. Furthermore, the fitness, fail-safe fitness, or fail-safe with redundancy fitness of the optimal sensor combinations with six sensors obtained by both search algorithms are close to each other. Thus, the GA adopted here is effective for searching out optimization results.

To check the performance of the sensor distributions obtained by the fail-safe SPO and the fail-safe with redundancy SPO, different histograms of the fitness values corresponding to all sensor distributions with the same number of sensors from an ES are also plotted in Figures 5–8 in green.

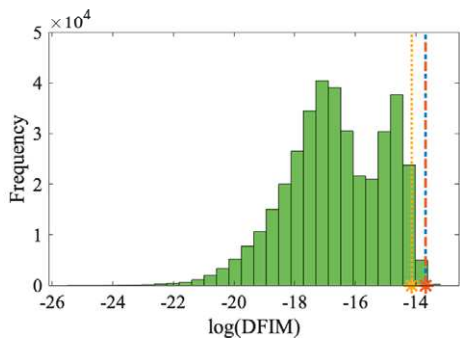
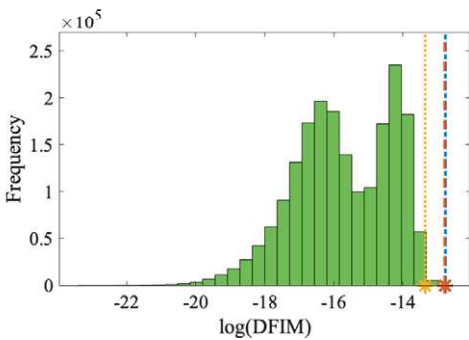
For the fail-safe SPO strategy, the expected result is that the performance of the sensor system before any sensor failure is very similar between the classical and fail-safe methods, while the worst-case performance of the sensor system obtained by the fail-safe method is better than that of the sensor system corresponding to the classical method after a critical sensor failure. This phenomenon can be observed particularly in four pairs of Figures 5a,b, 6c,d,e,f, and 8e,f.



(a) Before a sensor fails – four-sensor distributions. (b) After a sensor fails – three-sensor distributions.

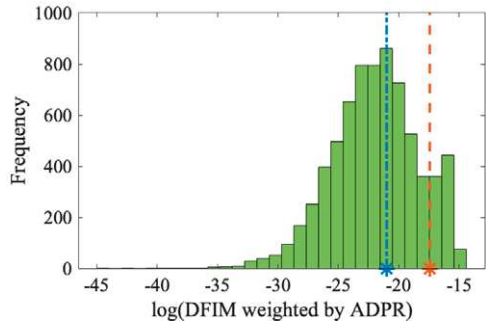
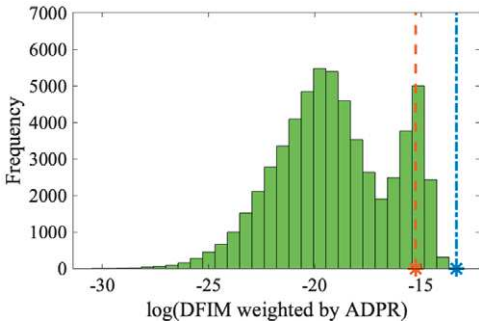


(c) Before a sensor fails – five-sensor distributions. (d) After a sensor fails – four-sensor distributions.

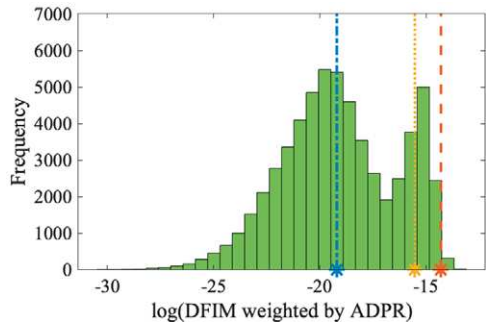
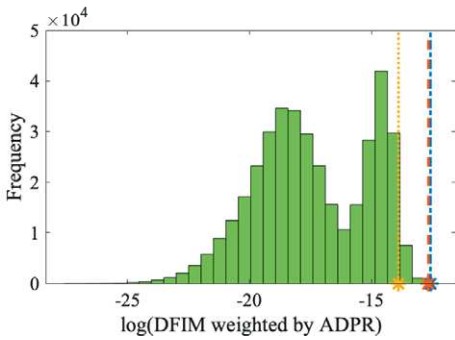


(e) Before a sensor fails – six-sensor distributions. (f) After a sensor fails – five-sensor distributions.

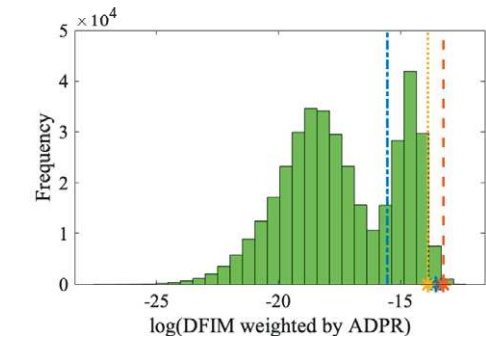
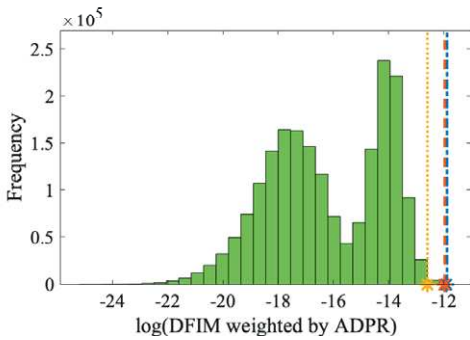
Figure 5. Comparison of the DFIM results of a GA, an improved-fail-safe GA, and an improved-fail-safe with redundancy GA, with the ES results.



(a) Before a sensor fails – four-sensor distributions. (b) After a sensor fails – three-sensor distributions.



(c) Before a sensor fails – five-sensor distributions. (d) After a sensor fails – four-sensor distributions.

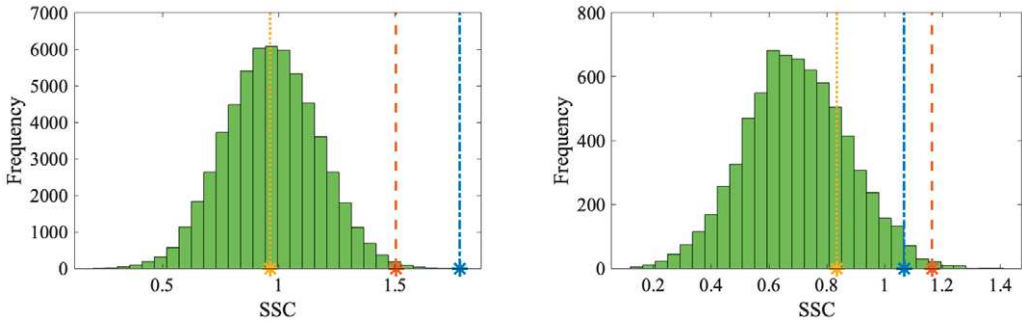


(e) Before a sensor fails – six-sensor distributions. (f) After a sensor fails – five-sensor distributions.

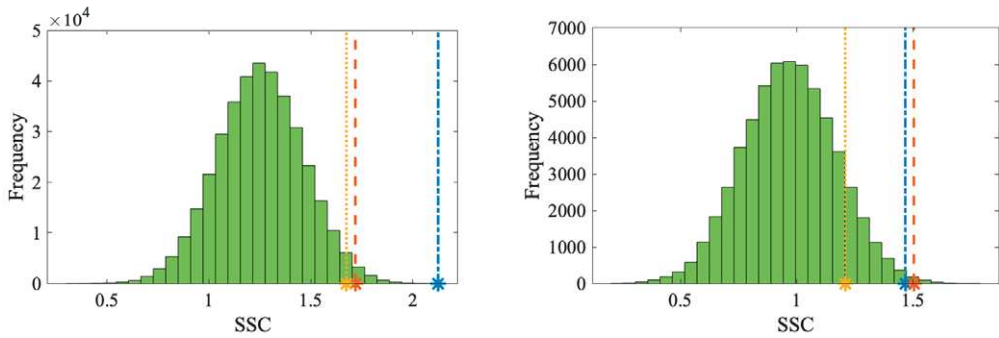
Figure 6. Comparison of the DFIM-ADPR results of a GA, an improved-fail-safe GA, and an improved-fail-safe with redundancy GA, with the ES results.

Overall, it can be found that the obtained improved-fail-safe sensor distribution provides good performance when all sensors are working normally. Besides, it also ensures that acceptable performance can be maintained when any sensor fails. For the case when the optimal improved-fail-safe sensor distribution (in orange) is the same as the optimal sensor distribution with the largest fitness (in blue), the obtained fail-safe sensor distribution does not compromise the system performance before any sensor fails, as demonstrated in Figures 5c,d and 8a,b.

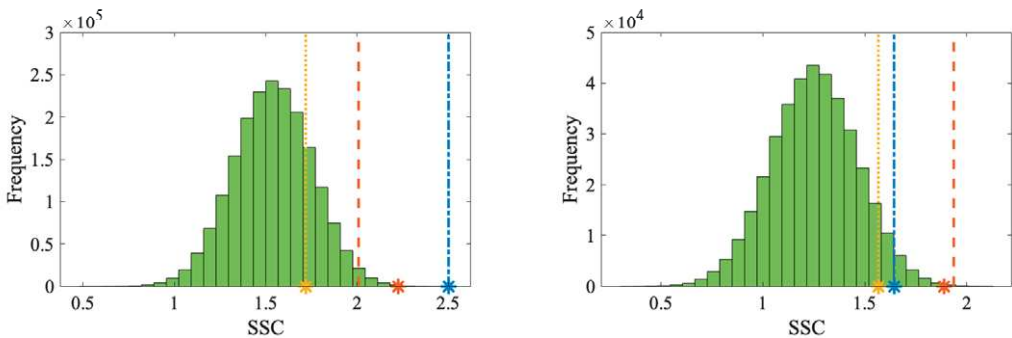
When it comes to the fail-safe with redundancy SPO, results in Figures 5–8 indicate that when the number of sensors is greater than 5, the performance corresponding to its optimal result changes the least before and after the sensor failure; this means that the redundant sensor is useful to increase the sensor system’s ability to withstand sensor failures. However, for this kind of SPO, a pair of sensors is placed at



(a) Before a sensor fails – four-sensor distributions. (b) After a sensor fails – three-sensor distributions.



(c) Before a sensor fails – five-sensor distributions. (d) After a sensor fails – four-sensor distributions.

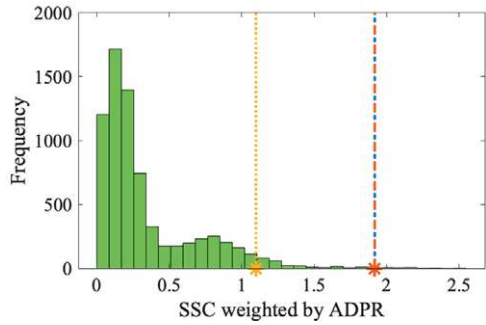
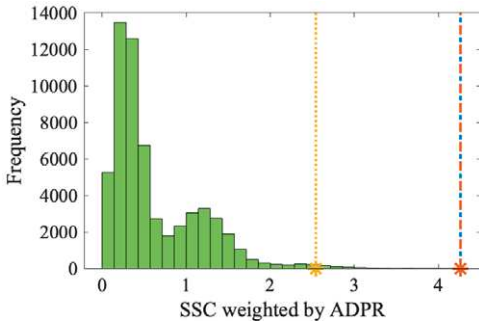


(e) Before a sensor fails – six-sensor distributions. (f) After a sensor fails – five-sensor distributions.

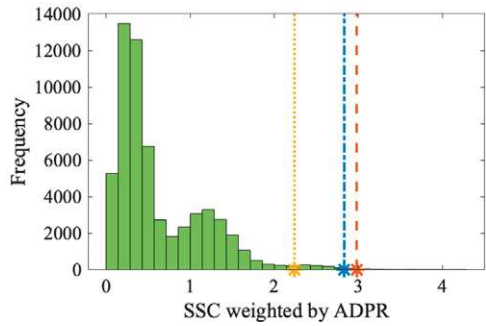
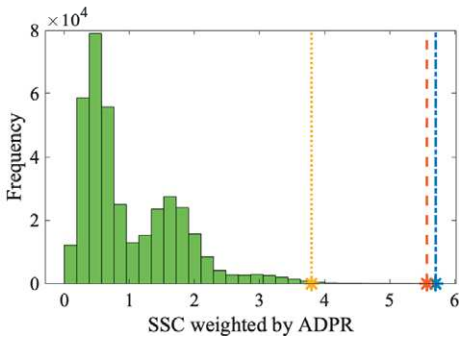
Figure 7. Comparison of the SSC results of a GA, an improved-fail-safe GA, and an improved-fail-safe with redundancy GA, with the ES results.

the same position, which will collect the same information. Therefore, although the sensor failure has the least effect on the performance of the sensor distribution, the optimal sensor distribution found via this optimization strategy almost always has the worst performance before and after a sensor fails compared with the other optimization approaches.

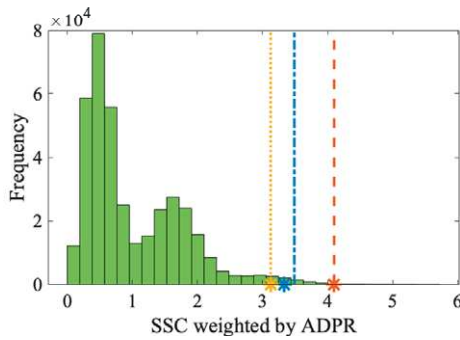
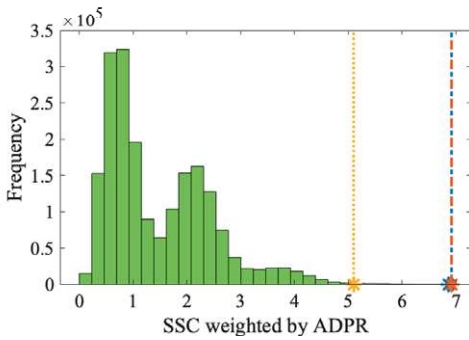
Note that the two improved fail-safe strategies cannot directly trade off the fitness of the mother distribution and the fail-safe fitness of the child distribution. Although the GA results in Figure 7e,f show the trade-off possibility, a possible reason for the phenomenon shown in Figure 7e,f is that the GA fails to find the optimal fail-safe sensor distribution, but instead finds a sub-optimal fail-safe sensor distribution, which sacrifices less performance of the sensor system without a failed sensor to consider the effect of sensor failure.



(a) Before a sensor fails – four-sensor distributions. (b) After a sensor fails – three-sensor distributions.



(c) Before a sensor fails – five-sensor distributions. (d) After a sensor fails – four-sensor distributions.



(e) Before a sensor fails – six-sensor distributions. (f) After a sensor fails – five-sensor distributions.

Figure 8. Comparison of the SSC-ADPR results of a GA, an improved-fail-safe GA, and an improved-fail-safe with redundancy GA, with the ES results.

5.4. Optimal sensor distribution comparisons

In this part, the optimal sensor distributions with six and eight sensors searched by an ES and a GA respectively are plotted in Figures 9 and 11 to analyze the distribution characteristics of sensors obtained using different optimization objectives. For each optimization objective, the sensor distributions obtained by the two search algorithms are similar. This phenomenon also reflects the reliability of GA results. So far, it can be said that a GA can be used to search for a reliable optimization result when optimizing a sensor system that is too complex for ES.

The specific features of optimal distributions included are as follows: (a) By comparing the optimal sensor distributions considering ADPR with the distribution of locations with larger ADPR values shown

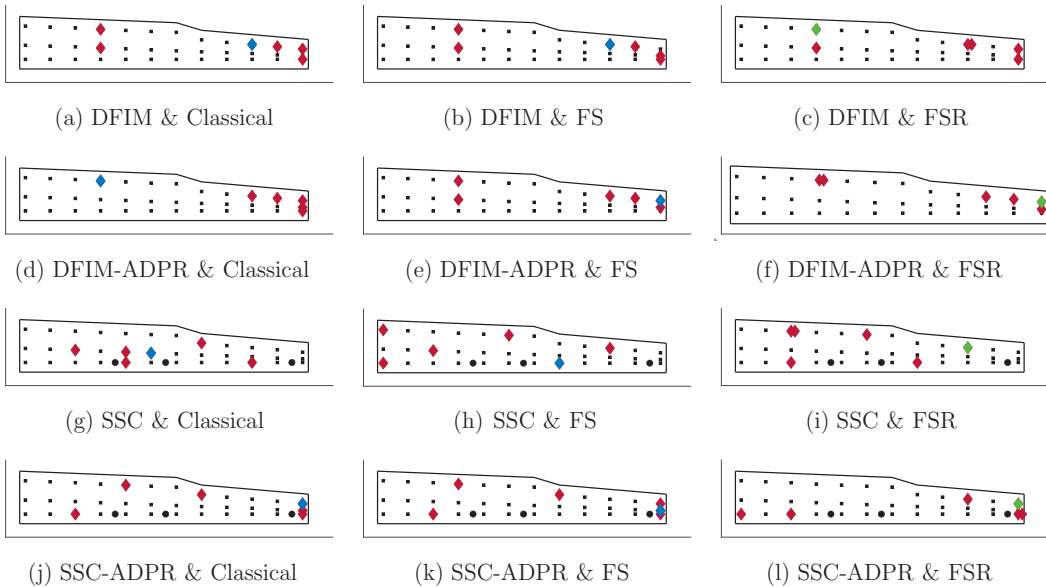


Figure 9. Comparison of optimal six-sensor distributions obtained by three ES-based optimization strategies combined with four optimization objectives. The selected sensor locations are marked in red. The sensors whose failure will lead to the worst and the second-worst child fitness are marked in blue and green. FR, fail-safe; FSR, fail-safe with redundancy.

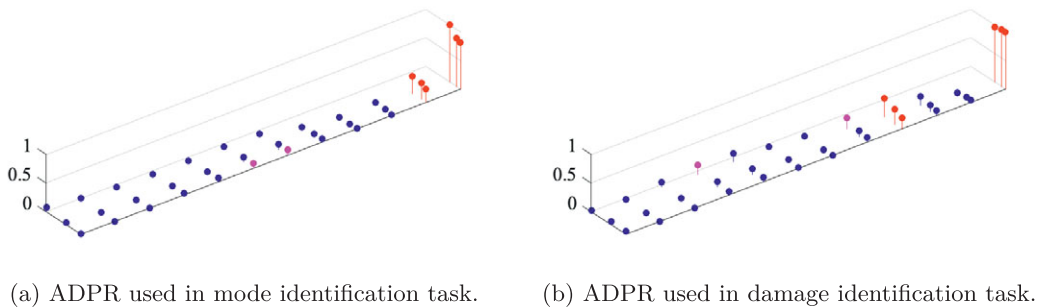


Figure 10. Rescaled ADPR corresponding to 36 candidate sensor locations. The first six maximum values are marked in red, and the next two are marked in magenta.

in Figure 10, it can be seen that the addition of signal strength in the fitness will have a certain impact on the result but it is limited. (b) Considering the signal strength in the objective function has a greater impact on the optimization results based on SSC than those based on DFIM. By comparing Figures 5 and 7, it can be seen that a possible reason for this phenomenon is that the difference in DFIM corresponding to different sensor combinations is larger than the difference in SSC. Therefore, the addition of ADPR into the optimization objective has a more limited impact on the ranking of DFIM-based fitness. (c) As expected, the optimal sensor distribution corresponding to SSC fitness is closer to the damage points of interest. (d) Fail-safe SPO makes the selected sensors more evenly dispersed on the structure to be monitored. This kind of deployment explains to a certain extent why the performance of the fail-safe sensor distribution is good, both before and after the sensor failure.

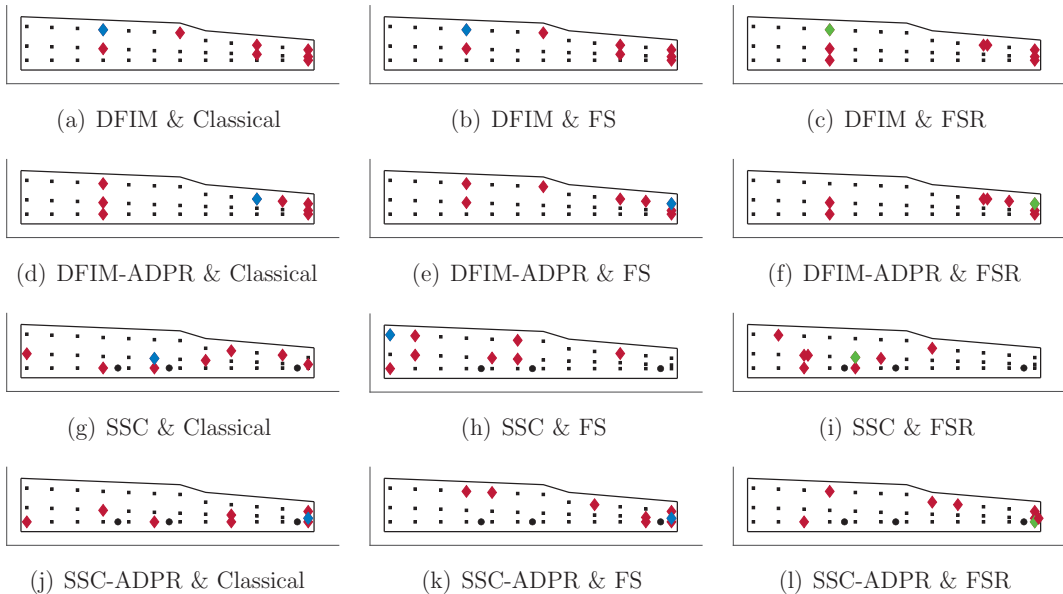


Figure 11. Comparison of optimal eight-sensor distributions obtained by three GA-based optimization strategies combined with four optimization objectives.

6. Conclusions

This article aims to design an optimization technique considering the effect of sensor failure for a wired sensor system. Two SPO strategies, including the improved-fail-safe SPO and the improved-fail-safe SPO with redundancy, are proposed for modal identification and damage identification issues. From three perspectives (the accuracy of the target modal-coordinate estimate, the vibration energy, and the information on the damage of interest), four objective functions based on model parameters, including the DFIM, the DFIM-ADPR, the SSC, and the SSC-ADPR, are adopted and combined with two search algorithms, including a deterministic algorithm—ES and a stochastic algorithm—GA to obtain the optimal sensor layouts. Among them, SSC is used as an optimization objective for sensor placement for the first time, which is inherently immune to the information redundancy and interaction issue.

A case study of a glider wing is demonstrated. By comparing with the classical SPO, it has been found that the improved-fail-safe sensor distribution can provide good performance when all sensors are working normally and guarantee good performance when any sensor fails. Furthermore, the redundant sensor helps enhance the sensor system's ability to withstand sensor failures, but the overall performance is not attractive; this shows that it is not advisable to place redundant sensors in a wired sensor system to avoid the worst system performance because of damage to a key sensor. In the case of a certain number of sensors, the improved fail-safe SPO can make the most effective use of sensor resources by placing the sensors in different locations.

In future work, in addition to mode shapes, other data types will be involved, including time-domain data and frequency-domain data, to further explore the feasibility and characteristics of the improved fail-safe SPO technique. If the data are suitable, the three optimization methods can be compared in the presence of uncertainty in the optimization process, and a cost-related optimization objective or multi-objective optimization can be considered. Cost-related evaluation studies could also be conducted in the future, to determine the number of sensors allowed to fail without any remedial action for a practical project.

Competing Interests. The authors declare no competing interests exist.

Acknowledgment. We thank Robin S. Mills for providing technical assistance for testing.

Supplementary Materials. To view supplementary material for this article, please visit <http://doi.org/10.1017/dce.2022.27>.

Data Availability Statement. The data and codes that support the findings of this study are openly available in the GitHub repository at https://github.com/TingnaW/Fail-safe_SPO_codes.

Author Contributions. Conceptualization: T.W., K.W.; Data curation: T.W., R.J.B.; Data visualization: T.W.; Formal analysis: T.W.; Funding acquisition: R.J.B., D.J.W., K.W.; Investigation: T.W.; Methodology: T.W., K.W.; Writing—original draft: T.W.; Writing—review and editing: T.W., D.J.W., K.W.

Funding Statement. The authors would like to acknowledge the support of Siemens Gamesa and UK EPSRC via grant number EP/R004900/1. This research made use of The Laboratory for Verification and Validation (LVV) which was funded by the EPSRC (grant numbers EP/J013714/1 and EP/N010884/1) and the University of Sheffield. For the purpose of open access, the author(s) has/have applied a Creative Commons Attribution (CC BY) licence to any Author Accepted Manuscript version arising.

References

- Abdollahzadeh S and Navimipour NJ** (2016) Deployment strategies in the wireless sensor network: A comprehensive review. *Computer Communications* 91–92, 1–16.
- Barthorpe RJ and Worden K** (2020) Emerging trends in optimal structural health monitoring system design: From sensor placement to system evaluation. *Journal of Sensor and Actuator Networks* 9(3), 31–51.
- Beck JV and Arnold KJ** (1977) *Parameter Estimation in Engineering and Science, Chapter 6*. New York: John Wiley & Sons, pp. 289–300.
- Bhuiyan MZA, Wang G, Cao J and Wu J** (2013) Deploying wireless sensor networks with fault-tolerance for structural health monitoring. *IEEE Transactions on Computers* 64(2), 382–395.
- Chen Z, Bao Y, Tang Z, Chen J and Li H** (2020) Clarifying and quantifying the geometric correlation for probability distributions of inter-sensor monitoring data: A functional data analytic methodology. *Mechanical Systems and Signal Processing* 138, 106540.
- Cox TF** (2005) *An Introduction to Multivariate Data Analysis, Chapter 22*. London: Hodder Education, pp. 141–143.
- Eiben AE and Smith JE** (2015) *Introduction to Evolutionary Computing*. Berlin/Heidelberg, Germany: Springer-Verlag.
- Eshghi AT, Lee S, Jung H and Wang P** (2019) Design of structural monitoring sensor network using surrogate modeling of stochastic sensor signal. *Mechanical Systems and Signal Processing* 133, 106280.
- Flynn EB and Todd MD** (2010) A Bayesian approach to optimal sensor placement for structural health monitoring with application to active sensing. *Mechanical Systems and Signal Processing* 24(4), 891–903.
- Hall MA** (1999) *Correlation-Based Feature Selection for Machine Learning*, PhD thesis. Hamilton, New Zealand: The University of Waikato.
- Hardoon DR, Szedmak S and Shawe-Taylor J** (2004) Canonical correlation analysis: An overview with application to learning methods. *Neural Computation* 16(12), 2639–2664.
- Hotelling H** (1936) Relations between two sets of variates. *Biometrika* 28(3/4), 321–377.
- Imamovic N and Ewins D** (1997) Optimization of excitation DOF selection for modal tests. In *Proceedings of the 15th International Modal Analysis Conference*, Society for Experimental Mechanics, Bethel, USA vol. 3089, pp. 1945–1951.
- Iqbal M, Naeem M, Anpalagan A, Ahmed A and Azam M** (2015) Wireless sensor network optimization: Multi-objective paradigm. *Sensors* 15(7), 17572–17620.
- Jaya MM, Ceravolo R, Fragonara LZ and Matta E** (2020) An optimal sensor placement strategy for reliable expansion of mode shapes under measurement noise and modelling error. *Journal of Sound and Vibration* 487, 115511.
- Kammer DC** (1991) Sensor placement for on-orbit modal identification and correlation of large space structures. *Journal of Guidance, Control, and Dynamics* 14(2), 251–259.
- Kammer DC** (1992a) Effect of model error on sensor placement for on-orbit modal identification of large space structures. *Journal of Guidance, Control, and Dynamics* 15(2), 334–341.
- Kammer DC** (1992b) Effects of noise on sensor placement for on-orbit modal identification of large space structures. *Journal of Dynamic Systems Measurement and Control—Transactions of the ASME* 114(3), 436–443.
- Krause A, Singh A and Guestrin C** (2008) Near-optimal sensor placements in Gaussian processes: Theory, efficient algorithms and empirical studies. *Journal of Machine Learning Research* 9(8), 235–284.
- Lu W, Wen R, Teng J, Li X and Li C** (2016) Data correlation analysis for optimal sensor placement using a bond energy algorithm. *Measurement* 91, 509–518.
- Middleton D** (1996) *An Introduction to Statistical Communication Theory, Chapter 22*. New York: Wiley-IEEE Press, p. 1012.
- Ostachowicz W, Soman R and Malinowski P** (2019) Optimization of sensor placement for structural health monitoring: A review. *Structural Health Monitoring* 18(3), 963–988.
- Papadimitriou C** (2004) Optimal sensor placement methodology for parametric identification of structural systems. *Journal of Sound and Vibration* 278(4–5), 923–947.

- Side S, Staszewski W, Wardle R and Worden K** (1997) Fail-safe sensor distributions for damage detection. In *Proceedings of the DAMAS 97*, Sheffield Academic Press, Sheffield, UK. pp. 135–146.
- Sun T and Chen S** (2007) Class label versus sample label-based CCA. *Applied Mathematics and Computation* 185(1), 272–283.
- Tan Y and Zhang L** (2020) Computational methodologies for optimal sensor placement in structural health monitoring: A review. *Structural Health Monitoring* 19(4), 1287–1308.
- Wang T, Wagg DJ, Worden K and Barthorpe RJ** (2021) On sensor optimisation for structural health monitoring robust to environmental variations. *Wind Energy Science* 6(5), 1107–1116.
- Worden K and Burrows AP** (2001) Optimal sensor placement for fault detection. *Engineering Structures* 23(8), 885–901.
- Yao L, Sethares WA and Kammer DC** (1993) Sensor placement for on-orbit modal identification via a genetic algorithm. *AIAA Journal* 31(10), 1922–1928.
- Yu L and Liu H** (2003) Feature selection for high-dimensional data: A fast correlation-based filter solution. In *Proceedings of the 20th International Conference on Machine Learning (ICML-03)*, pp. 856–863.
- Zhang S and Lang Z-Q** (2022) Orthogonal least squares based fast feature selection for linear classification. *Pattern Recognition* 123, 108419.